NASA Technical Memorandum 85799

TENSION WAVES IN TETHERED SATELLITE CABLES

Frederick J. Lallman

May 1984

National Aeronautics and
Space Administration

Langley Research Center
Hampton, Virginia 23665

TENSION WAVES IN TETHERED SATELLITE CABLES

Frederick J. Lallman
NASA Langley Research Center
Hampton, Virginia

SUMMARY

A one-degree-of-freedom simulation of the Tethered Satellite System (TSS) was programed using a distributed system model of the tether based on the one-dimensional wave equation. This model represents the time varying tension profile along the tether as the sum of two traveling waves of tension moving in opposite directions. A control loop was devised which combines a deployment rate command with the measured tension at the deployer to produce a smooth, stable rate of deployment of the subsatellite. Simulation results show a buildup of periodic bursts of high frequency oscillation in tension. This report covers the mathematical modelling and simulation results and explains the reason for the observed oscillations. The design of a possible vibration damping device is discussed.

INTRODUCTION

The concept of the Tethered Satellite System (TSS) is to deploy a small (500 kg) subsatellite from a deployer located in the cargo bay of the Space Shuttle Orbiter to distances up to 100 km. The subsatellite remains attached to the shuttle by means of a fine (1-3 mm/diameter) tether. The system utilizes gravity gradient to hold the tether taut and provides static stability about the local vertical. Control of the system is provided by means of gas jets on the subsatellite and by regulation of the deployed tether length. Additional details may be found in references 1 and 2.

Simulations of tethered satellite systems have been conducted by several investigators. These simulations have been approached by either the technique of generalized coordinate analysis (See Ref. 3, for example) or by finite elements analysis (See Ref. 4, for example). Another approach is to apply transmission line theory to model the dynamics of the tether (Ref. 5). This paper describes a one-degree-of-freedom simulation of the TSS utilizing the latter approach.

SYMBOLS

A	cross sectional area, m^2
a,b	defined by equations (24) and (25), respectively
c	speed of propagation of tension waves, m/s
D	damping coefficient, Ns/m

E	modulus of elasticity, Pa
k	spring constant, N/m
L	length of tether, m
m	mass, kg
s	Laplace transform variable, sec^{-1}
T	tension, N
t	time, sec
x	displacement of point on tether, m
z	location of point on unstressed tether, m
ρ	mass density, kg/m^3
ω	frequency of oscillation, rad/sec
ω_c	natural frequency of vibration damper, equals $\sqrt{k_v/m_v}$, rad/sec
ω_1,ω_2	frequencies for which vibration damper has 50 percent attenuation, rad/sec

Subscripts

t	tension sensor
v	vibration damper
1	variable value at deployer end of the tether
2	variable value at subsatellite end of the tether
+	denotes wave motion in the direction of increasing z
-	denotes wave motion in the direction of decreasing z

Miscellaneous

A prime (') denotes the derivative with respect to the argument shown.
A dot (•) over a variable denotes the derivative with respect to time.
One decibel (db) is 20 times the logarithm to the base ten.

TETHER DYNAMIC MODEL

The tether is considered to be a uniform length of elastic, massive material as is depicted in figure 1. The location of each point along the length of the undeformed tether is denoted by the value of the independent variable z. Given a dynamic deformation, each point is displaced a distance $x(z,t)$. The tension created by the deformation is a function of the strain of the material.

$$T(z,t) = EA \frac{\partial}{\partial z} x(z,t) \tag{1}$$

where E is the elastic modulus, Pa
A is the cross-sectional area, m^2

The acceleration of an infinitesimal section of the tether is a function of the tension acting on either side of the section. This can be expressed as

$$\frac{\partial^2}{\partial t^2} x(z,t) = \frac{1}{\rho A} \frac{\partial}{\partial z} T(z,t) \tag{2}$$

where ρ is the mass density, kg/m^3

Combining equations (1) and (2) yields the one-dimensional wave equation of the tether

$$\frac{\partial^2}{\partial t^2} x(z,t) - c^2 \frac{\partial^2}{\partial z^2} x(z,t) = 0 \tag{3}$$

$$c = \sqrt{\frac{E}{\rho}} \tag{4}$$

Following d'Alembert's solution of the wave equation (Ref. 6), the displacement of each point along the tether may be written as

$$x(z,t) = x_+ (z-ct) + x_- (z+ct) \tag{5}$$

where x_+ is a spatial function which travels (to the right on Fig. 1) at the phase velocity of c, and

x_- is a similar function which travels in the opposite direction.

The tension at each point along the tether is found by substituting equation (1) into equation (5).

$$T(z,t) = EA [x'_+ (z-ct) + x'_- (z+ct)] \tag{6}$$

where the primes denote derivatives with respect to the entire arguments z-ct and z+ct, respectively.

The velocity of each point along the tether is found by differentiating equation (5) with respect to time.

$$\dot{x}(z,t) = \sqrt{\frac{E}{\rho}} [-x'_+ (z-ct) + x'_- (z+ct)] \tag{7}$$

Since the functions x_+ and x_- are independent of each other, the tether dynamics may be described by waves of tension and velocity.

$$T(z,t) = T_+ (z-ct) + T_- (z+ct) \tag{8}$$

$$\dot{x}(z,t) = \dot{x}_+ (z-ct) + \dot{x}_- (z+ct) \tag{9}$$

The tension and velocity waves are proportionally related.

$$T_+(z-ct) = -A\sqrt{\rho E}\ \dot{x}_+(z-ct) \tag{10}$$

$$T_-(z+ct) = +A\sqrt{\rho E}\ \dot{x}_-(z+ct) \tag{11}$$

The effect of the traveling waves at different locations along the tether (different values of z) are related by a time delay equal to the distance between the locations divided by the phase velocity, c. Using the subscript 1 to denote the values of the traveling waves at z=0 (the left end of the tether in Fig. 1) and the subscript 2 to denote the values of the waves at z=L (the right end), the following equations may be written

$$T_1(t) = T_{1+}(t) + T_{1-}(t) \tag{12}$$

$$\dot{x}_1(t) = \dot{x}_{1+}(t) + \dot{x}_{1-}(t) \tag{13}$$

$$T_2(t) = T_{2+}(t) + T_{2-}(t) \tag{14}$$

$$\dot{x}_2(t) = \dot{x}_{2+}(t) + \dot{x}_{2-}(t) \tag{15}$$

where

$$T_{2+}(t) = T_{1+}\left(t - \frac{L}{c}\right) \tag{16}$$

$$T_{1-}(t) = T_{2-}\left(t - \frac{L}{c}\right) \tag{17}$$

$$\dot{x}_{2+}(t) = \dot{x}_{1+}\left(t - \frac{L}{c}\right) \tag{18}$$

$$\dot{x}_{1-}(t) = \dot{x}_{2-}\left(t - \frac{L}{c}\right) \tag{19}$$

and where L is the length of the tether, m.

Therefore, the influences of the traveling waves at the ends of the tether are related through transport delays. A disturbance originating at one end propagates along the length of the tether and appears at the other end delayed by the time interval of duration L/c. Given that the ends of the tether are attached to bodies whose motions are known, equations (13) and (15) describe the boundary conditions. Transforming these into terms of tension waves by equations (10) and (11) yields

$$T_{1+}(t) = T_{1-}(t) - A\sqrt{\rho E}\,\dot{x}_1(t) \tag{20}$$

$$T_{2-}(t) = T_{2+}(t) + A\sqrt{\rho E}\,\dot{x}_2(t) \tag{21}$$

These relationships indicate that the traveling tension waves emanating from the ends of the tether are composed of reflections of the waves impinging on the ends plus components which are proportional to the velocities of the attached bodies.

In summary, the dynamic behavior of the elastic, massive tether is described by waves traveling in either direction along the tether. The values of these waves at the ends of the tether are related through transport delays in equations (16) and (17). The boundary conditions of equations (20) and (21) give the relationships between the forced motions of the ends of the tether and the traveling waves. The forces that the tether apply to the attached bodies are given by equations (12) and (14). These relationships define the dynamic model of the tether depicted in figure 2.

SIMULATION TEST

A feedback control system was devised and simulated in conjunction with the tether dynamic model developed above for the purpose of exploring for any possible stability problems which might be caused by the transport delays inherent in the tether. The requirement of the control system is to deploy the tether, which has an inert mass suspended from the end, at a commanded rate in a smooth and stable manner. This was accomplished by combining the commanded rate with a sensed value of the tension in the tether near the deployer to form a drive signal for the deployer mechanism. The general arrangement of the system is given in figure 3. The parameter values used in the simulation are given in table 1. The arrangement of the control system and the values used were selected by the author and represent only a rough approximation of the actual TSS system.

The deployer mechanism consists of a spool upon which the undeployed portion of the tether is stored, a motor which causes the tether to be reeled in and out, a spring-mounted pulley whose position is a measure of the tension in the tether, and an electronic control network. The motor and spool mechanism is modeled as a second order system with natural frequency of 10 r/s and damping ratio of 0.7. The tension sensing device is modeled as a mass-spring-damper system for which the values of table I give a natural frequency of 31.6 r/s and a damping ratio of 0.16. The extension of the spring is used as a measure of the tension in the tether. This might be accomplished in practice by using a load cell attached to the fixed end of the spring. The translation of the pulley also affects the deployed length of the

tether. The sensed tension is passed through a washout filter to block slow variations in the tension caused by gravity gradient force changes and libration motions. The feedback gain chosen gives a closed loop frequency of .046 r/s and damping ratio of 0.53 based upon a lumped-parameter model of the tether as an ideal spring. A command prefilter is used to provide smooth operation of the system in response to commanded rate changes.

The simulation model was programed on a hybrid computer in LaRC's Aerospace Controls Research Lab. The motions of the load mass and the dynamics of the deployer mechanism and the control system were simulated on an analog computer. The transmission line model of the tether was implemented on a digital computer operating at 100 samples per second. Since the tether simulation model of figure 2 includes a loop which has unity gain, tension waves started in this model will circulate continuously until they are cancelled by motions of the deployer or the subsatellite. During the simulations, this model accumulated a background signal consisting of very high frequency noise up to 50 Hz (one half the sample frequency or 314 r/s) which is well outside the bandwidth of the controller and the subsatellite. Since this did not affect the present study, no corrective action was taken. For applications where longer simulation times are required (10 minutes or more), some means to attenuate this high frequency noise within the loop will be necessary.

The simulated time histories of the system to a step command rate of 18.3 m/s are given in figure 4. The subsatellite initially is considered to be deployed in a stable vertical condition with a tether length of 100 km. Given a subsatellite mass of 500 kg, the steady state tension in the tether caused by the gravity gradient is 400 N. Because of the finite propagation rate of disturbances along the tether, there is a 10 second delay between the time of deployer activation and reaction of the subsatellite. There is an additional 10 second delay before the reaction of the subsatellite is felt at the deployer. During the first 20 seconds, the deployer reaches a steady rate of 12.2 m/s and the tension in the tether has dropped by 133 N. At 10 seconds the tension wave reaches the subsatellite and is reflected, thus doubling its effect upon the subsatellite. As the subsatellite moves, the tension acting upon it decreases in proportion to the subsatellite velocity. At 20 seconds the tension wave which was reflected from the subsatellite returns to the deployer and further decreases the sensed tension. The control loop responds by decreasing the deployment rate. As time progresses, the staircasing type of behavior of the tension diminishes and the system response approaches that of the idealized lumped-parameter approximation. The subsatellite smoothly reaches the commanded rate after about 1 minute with a small overshoot. However, there now appears a periodic disturbance in the tension of the tether. An expanded view of this disturbance after 2 1/2 minutes of operation is given in figure 5. The disturbance appears as a short burst of high frequency sinusoidal oscillations. The oscillation frequency is about 13.3 r/s which is higher than the natural frequency of the actuator. The repetition rate of the disturbance is about 20 seconds which is twice the length of the tether divided by the speed of propogation of tension waves. The magnitude of the disturbance increases by 38 percent (2.8 db) for successive occurrences.

Several modifications of the control system were made in an attempt to eliminate the disturbance:

1. The dynamic model of the tension sensor was removed and the actual tension was used.

2. The actuator was changed to have a first order characteristic; then it was changed to be ideal.

3. A low-pass filter was inserted in the feedback loop.

In each trial, the frequency of oscillation of the disturbance changed and/or the rate of growth was changed, but it was not eliminated. However, the combination of ideal sensing of the tension with a first order actuator model did eliminate the disturbance completely. But this is a severe over-simplification which is not valid for examining the real system behavior.

ANALYSIS

This section outlines the analysis which was performed to determine the reasons for occurrence of the vibration phenomenon observed in the simulation test. Using equations (12) and (20), the transfer function of the tension wave emanating from the deployer, T_{1+}, as a result of the incoming wave, T_{1-}, conditioned by the action of the feedback loop was derived.

$$\frac{T_{1+}}{T_{1-}}(s) = \frac{1 - A\sqrt{\rho E}\ \left[\frac{\dot{x}_1}{T_1}(s)\right]}{1 + A\sqrt{\rho E}\ \left[\frac{\dot{x}_1}{T_1}(s)\right]} \tag{22}$$

where $\frac{\dot{x}_1}{T_1}(s)$ is the transfer function of the deployer including the tension sensor, the actuator, and the feedback network. Replacing s by $i\omega$ and then writing the deployer transfer function as the sum of its real and imaginary parts yields the ratio of the magnitude of reflected waves to the magnitude of incident waves.

$$\left|\frac{T_{1+}}{T_{1-}}(\omega)\right| = \left[1 - \frac{4a(\omega)}{[1+a(\omega)]^2 + [b(\omega)]^2}\right]^{1/2} \tag{23}$$

where

$$a(\omega) = \frac{1}{A\sqrt{\rho E}}\ \mathrm{Re}\left[\frac{\dot{x}_1}{T_1}(\omega)\right] \tag{24}$$

$$b(\omega) = \frac{1}{A\sqrt{\rho E}}\ I_m\left[\frac{\dot{x}_1}{T_1}(\omega)\right] \tag{25}$$

The ratio given by equation (23) is greater than unity if the real part of the transfer function of the control system is less than zero ($a(\omega) < 0$). The tangent of the phase angle of the control system is the imaginary part of its transfer function divided by the real part or $b(\omega)/a(\omega)$. If the real part is negative, then the phase angle lies in the second or third quadrant. At those frequencies where the phase angle of the control system is outside the range of -90° to +90°, equation (23) is greater than unity. Reflected waves at these frequencies will be larger than the incident waves.

The value of equation (23) for the simulated system is plotted in figure 6 (the solid curve). The reflection of tension waves at the deployer results in amplification in the frequency range of 9.35 r/s to 27.9 r/s with the peak gain of 2.84 db (39 percent increase) occurring for a frequency of 16.2 r/s. These values agree closely with the observed phenomenon.

Since the tension sensor has second order dynamics and the actuator has at least first order dynamics and in any real system there are many sources for unmodeled lags, the analysis of this section indicates that there will be amplification of tension waves at the deployer. The addition of filters in the control loop to suppress the control activity at the frequencies of interest is possible, but the type of oscillation observed will recur at a different frequency. This being the case, attenuation of the phenomenon must be accomplished by means other than control law modifications.

Dispersion

The deficiency of the tether dynamic model used in the present study is that there is no accounting for dispersion. The effects of dispersion are (1) waves of different frequencies may propagate at different velocities, and (2) waves at some frequencies may be attenuated as they propagate along the tether. If the latter effect is present, the amplitude of a traveling wave at a given frequency will decrease as an exponential function of the distance travelled. If there is sufficient attenuation of the waves as they make the two-way journey along the deployed length of the tether to offset the amplification of the reflection at the deployer, then the vibration phenomenon will tend to die out. If there is sufficient attenuation in the tether during the initial deployment and final retrieval phases (length on the order of 2 km), then there will be ample attenuation at longer deployed lengths. Since the dispersion characteristics of the candidate tethers were not known at the time of this study, only the worst case (dispersion equals zero) was considered. See reference 5 for further information about the effects of dispersion.

Tension Sensor Damping

The value of the damping coefficient used in the simulation (40 Ns/m) was changed to determine the effect of this parameter upon the vibration phenomenon. Using equation (23), it was observed that deletion of the damping coefficient altogether results in peaking near the natural frequency of the tension sensor mechanism (See Fig. 6). Increasing the coefficient to 200 Ns/m results in peaking near the natural frequency of the actuator. Neither change made any improvement over the original system. In addition, significant increase in this damping may impair the ability of the tension sensor to follow the tether and allow the tether to become slack and possibly foul the deployer mechanism. Moreover, the stresses experienced by the tether when it is pulled taut again may be quite high and unpredictable.

VIBRATION DAMPER

A number of modifications to the end of the tether where it attaches to the subsatellite were made in an attempt to discover a means of dealing with the vibrations there. In one attempt, a portion of the tether near the end was changed to a larger diameter. In another attempt, an idealized spring was inserted at the attachment point. Neither modification caused any attenuation, only frequency-dependent phase shifts. The insertion of a mass-spring-damper combination shown in figure 7a at the end of the tether was found to provide the desired attenuation. An analysis of this arrangement follows.

Using equations (14) and (21), the transfer function of the tension wave emanating from the subsatellite end of the tether, T_{2-}, resulting from the reflection of the impinging wave, T_{2+}, conditioned by the dynamics of the load and the inserted vibration damper was derived.

$$\frac{T_{2-}}{T_{2+}}(s) = \frac{1 + A\sqrt{\rho E}\ \frac{\dot{x}_2}{T_2}(s)}{1 - A\sqrt{\rho E}\ \frac{\dot{x}_2}{T_2}(s)} \tag{26}$$

where $\frac{\dot{x}_2}{T_2}(s)$ is the transfer function of the load on the tether including the subsatellite and the vibration damper. Note that the reflections are zero if

$$\frac{\dot{x}_2}{T_2}(s) = \frac{1}{A\sqrt{\rho E}} \tag{27}$$

which is the equation of a viscous damper anchored in space.

Since this is physically unrealizable, the suggested vibration damper of figure 7a was chosen as a reasonable alternative. The subsatellite is considered to be immobile in the frequency range of interest for the following development. Maximum attenuation occurs at the natural frequency of the vibration damper and the ratio of the reflected wave to the incident wave at this frequency is

$$\left| \frac{T_{2-}}{T_{2+}}\left(\omega = \sqrt{\frac{k_v}{m_v}}\right) \right| = \left| \frac{D_v - A\sqrt{\rho E}}{D_v + A\sqrt{\rho E}} \right| \tag{28}$$

where m_v, k_v, and D_v are the mass, spring constant, and viscous damping coefficient of the vibration damper, respectively. For other frequencies, tension waves are attenuated to lesser amounts depending on the proximity of their frequency to the natural frequency of the vibration damper as shown in figure 7b. In order to obtain a measure of the effective bandwidth of the vibration damper, the frequencies at which the amplitudes of reflected waves are one half the amplitudes of the incident waves were calculated. These frequencies (ω_1 and ω_2 on Fig. 7b) are given by the following formula.

$$\frac{\omega^2}{k_v/m_v} = \left(1 + \frac{2}{3}\frac{A^2\rho E}{k_v m_v}\right) \pm \sqrt{\left(1 + \frac{2}{3}\frac{A^2\rho E}{k_v m_v}\right)^2 - 1} \qquad (29)$$

where the damping coefficient, D_v, has been matched to the characteristic "impedance" of the tether, $D_v = A\sqrt{\rho E}$, which gives complete attenuation at the natural frequency of the vibration damper. The solutions of equation (29) are plotted in figure 7c.

The bandwidth of the vibration damper is a function of the product of its spring constant and mass, $k_v m_v$. The effective frequency range is centered (in the logarithmic sense) on its natural frequency, $\sqrt{k_v/m_v}$. The effective frequency range is broad for low values of $k_v m_v$ and narrow for high values. Small values of mass, m_v, are desirable to minimize the weight penalty involved in adding the vibration damper to the system. Large values of spring constant, k_v, are desirable to limit its physical size if the vibration damper is to function over a wide range of steady state tension. If a high spring constant is selected, then a large mass is required to tune the vibration damper to the frequency of the vibrations to be damped. This in turn results in a narrow bandwidth. In practice, there is a tradeoff to be made between the length and the weight of the vibration damper and its effective bandwidth.

The effectiveness of a candidate vibration damper was investigated. The value of the damping coefficient was matched to the impedance of the tether, 10.95 Ns/m, the mass was chosen to be .79 kg, and the spring constant was chosen to be 316 N/m. These values result in 100 percent attentuation at 20 r/s and 50 percent attenuation (-6 db) at 13.5 r/s and 29.5 r/s. Combining the transfer function of the wave reflections at the deployer with the transfer function at the vibration damper yields the overall gain of the traveling waves as they make the round trip along the tether. This gain, plotted as the solid curve in figure 8, indicates that the vibration damper will attenuate the vibrations sufficiently to overcome their amplification at the deployer. However, the vibration damper does not have sufficient bandwidth to be effective if the damping coefficient of the tension sensor is reduced to zero or increased to 200 Ns/m (see the broken curves in Fig. 8).

The simulation test described in a previous section was repeated with the vibration damper included. The time histories are given in figure 9. The response of the system to step commanded rate is identical to the previous simulation (see Fig. 4) but with no evidence of high frequency vibrations. Such vibrations were artificially introduced, and they were seen to damp out in the presence of the vibration damper.

Since the nominal tension in the tether is 400 N, the selected spring is stretched by 1.3 meters by the steady-state tension. This implies that the overall length of the vibration damper might approach 3 meters during transients. This may be excessive for the intended application. It is conceivable that the vibration damper might be mechanized by a spring-loaded rotating drum which is connected to a rotary damper. Such an arrangement could be made in a small package, but this idea needs further study.

Another topic of further study would be to increase the damping coefficient, D_V, above the value used in the above analysis. This would broaden the effective bandwidth of the vibration damper while sacrificing the peak level of attenuation achieved. This change would result in a larger mass and higher spring constant and would allow for a smaller physical overall length. Such a design might be better able to accommodate tethers of different sizes and material properties.

CONCLUDING REMARKS

A study of the dynamic behavior tension waves in the cable of a tethered satellite system has been conducted. The tether dynamics were modeled by a one-dimensional wave equation whose solution is described by traveling waves of tension moving in either direction along the tether. The subsatellite was modeled as an inert mass suspended by the tether from the main satellite. Aboard the main satellite there is a deployer mechanism which includes a motorized reel mechanism, a tension sensing device, and control electronics. The control electronics combine the commanded rate with a sensed value of the tension in the tether near the deployer to form a drive signal for the deployee mechanism.

The system was simulated using a model of the tether dynamics which includes transport delays to represent the finite time it takes for actions occurring at one end of the tether to effect reactions at the other end. The simulation showed a buildup of bursts of high frquency oscillation of the tension in the tether. The cause of this phenomenon was determined to be amplification of certain frequencies of tension waves as they are reflected at the deployer. This occurs whenever the phase angle of the control loop between the sensed tension and the deployment rate exceeds 90°. No reasonable alterations to the control law or to the tension sensing device were found which could eliminate this behavior.

Since the dissipation characteristics of traveling waves in the tether were not available for this study, it could not be determined whether dispersion would sufficiently attenuate the vibrations to overcome this problem. If the dissipative nature of the tether were known, it should be noted that the associated attenuation is an exponential function of tether length and may be effective only at long tether lengths.

It was found that a mass-spring-damper system added to the end of the tether where the subsatellite is attached could be effective in eliminating the vibrations. In the design of this device, the values of the mass and spring would be selected so that their natural frequency would match the center frequency of the vibrations, the value of the damper coefficient would equal the "characteristic impedance" of the tether, and the product of the mass and spring constant would be selected to provide sufficient bandwidth to attenuate the range of frequencies involved in the vibrations. A tradeoff must be made between the size of the mass and the spring constant to minimize the weight penalty and the length of the vibration damper while maintaining sufficient attenuation of the vibrations.

REFERENCES

1. Bekey, Ivan: Tethers Open New Space Options. Astronautics and Aeronautics, April 1983, pp. 32-40.

2. Banejee, Arun K.; and Kane, Thomas R.: Tethered Satellite Retrieval with Thruster Augmented Control. Journal of Guidance, Vol. 7, No. 1, Jan-Feb 1984, pp. 45-50.

3. Mesra, A. K.; and Modi, V. J.: Deployment and Retrieval of Shuttle Supported Tethered Satellites. Journal of Guidance, AIAA 80-1693R, Vol. 5, No. 3, May-June 1982, pp. 278-285.

3. Kalaghan, P. M., et al.: Study of the Dynamics of a Tethered Satellite System (Skyhook). NASA CR-150719, March 1978.

5. Flotow, A. H.: A Traveling Wave Approach to the Dynamic Analysis of Large Space Structures. AIAA Paper No. 83-0964, 24th Structures, Structual Dynamics and Materials Conference, Lake Tahoe, NY, May 2-4, 1983, pp. 509-519.

6. Kreysig, Erwin: Advanced Engineering Mathematics. John Wiley & Sons, Inc., 1962, pp. 536-537.

TABLE 1 - PARAMETER VALUES USED IN SIMULATION

Tether	
Diameter	1mm
Mass Density	1440 kg/m^3
Elastic Modulus	135 GPa
Length	100 km
Deployer Actuator	
Natural Frequency	10 r/s
Damping Ratio	.7
Tension Sensor	
Spring Constant	4000 N/m
Mass	4 kg
Damping Coefficient	40 Ns/m
Command Prefilter	
Break Frequency	1 r/s
Washout Filter	
Time Constant	200 sec
Suspended Body	
Mass	500 kg
Feedback	
Gain	.0457 m/Ns

$$T(z,t) = EA \frac{x(z+dz,\ t) - x(z,\ t)}{dz}$$

$$\rho A\, dz \frac{\partial^2}{\partial t^2} x(z,\ t) = T(z+dz,\ t) - T(z,\ t)$$

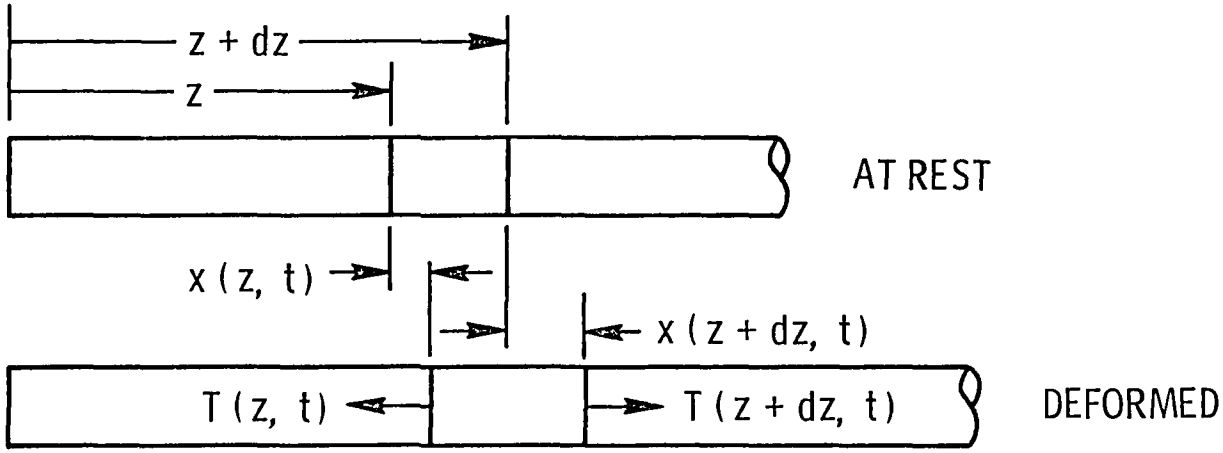

$$\frac{\partial^2}{\partial t^2} x(z,t) - \frac{E}{\rho} \frac{\partial^2}{\partial z^2} x(z,\ t) = 0$$

NOTE: DISPLACEMENTS SHOWN ARE POSITIVE

Figure 1.- Elastic Deformation Dynamics

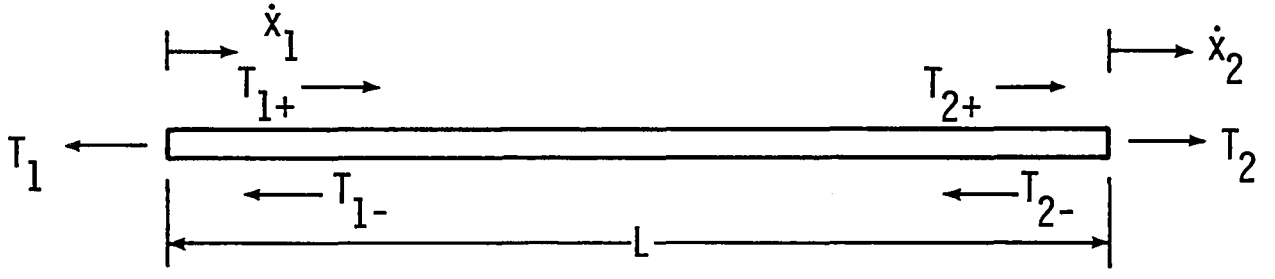

a) Physical Model

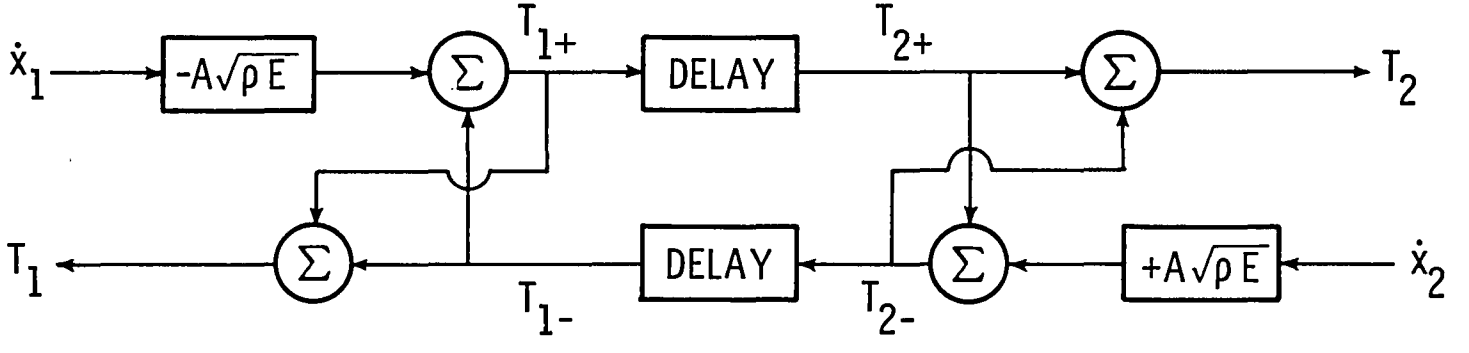

DELAY TIME = L/c

$$C = \sqrt{\frac{E}{\rho}}$$

b) Flow Diagram

Figure 2.- Elastic Tether Simulation Model

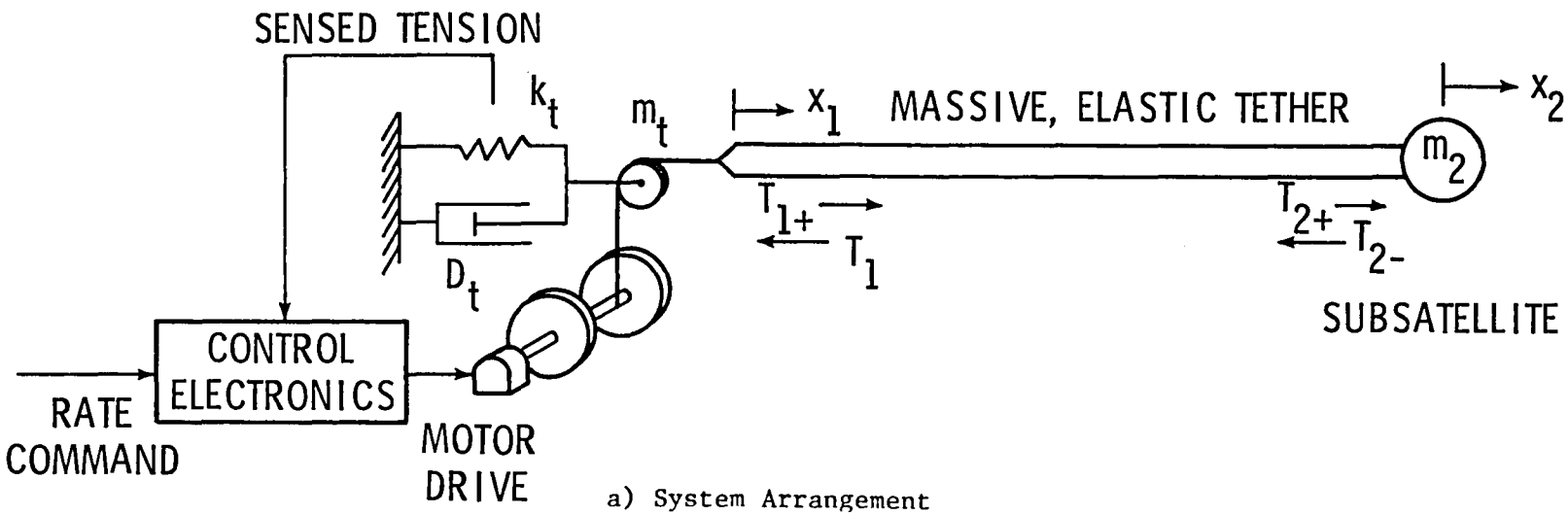

a) System Arrangement

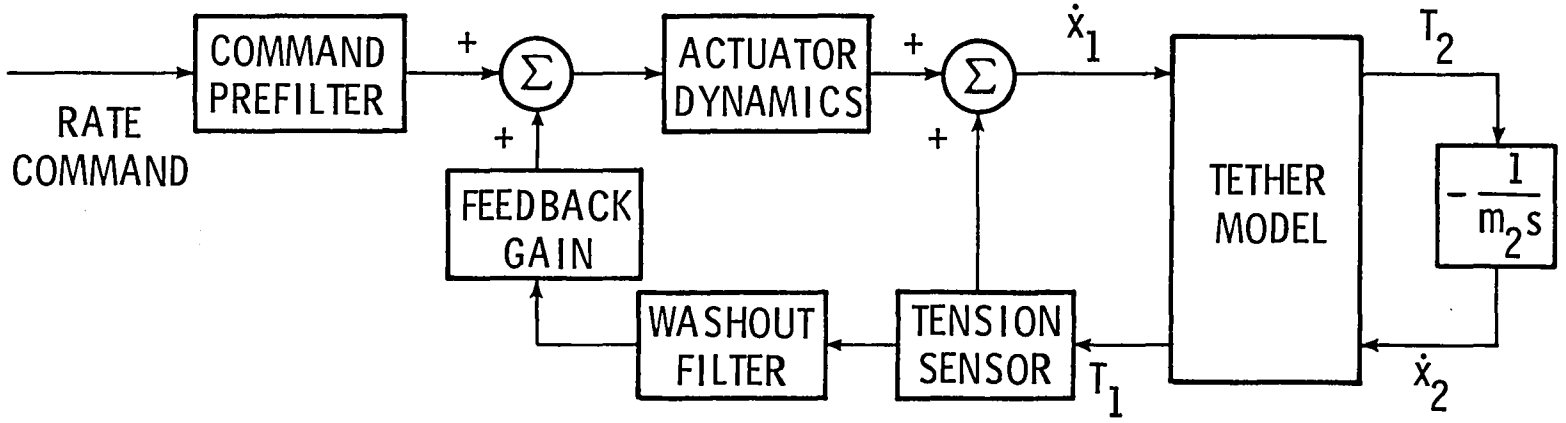

b) Signal Flow Diagram

Figure 3.- Tethered Satellite Simulation Model

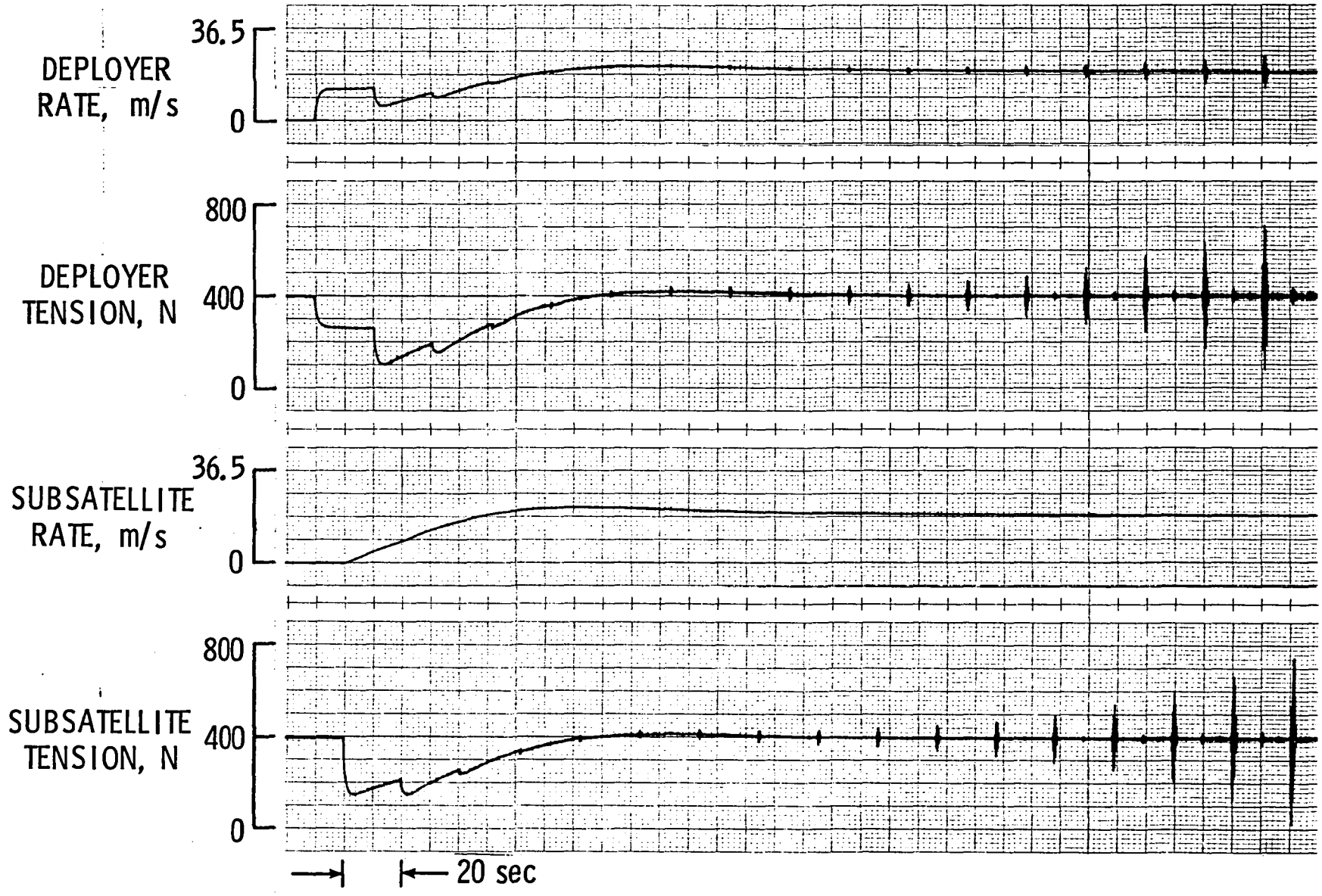

Figure 4.- Simulated Tethered Satellite Deployment

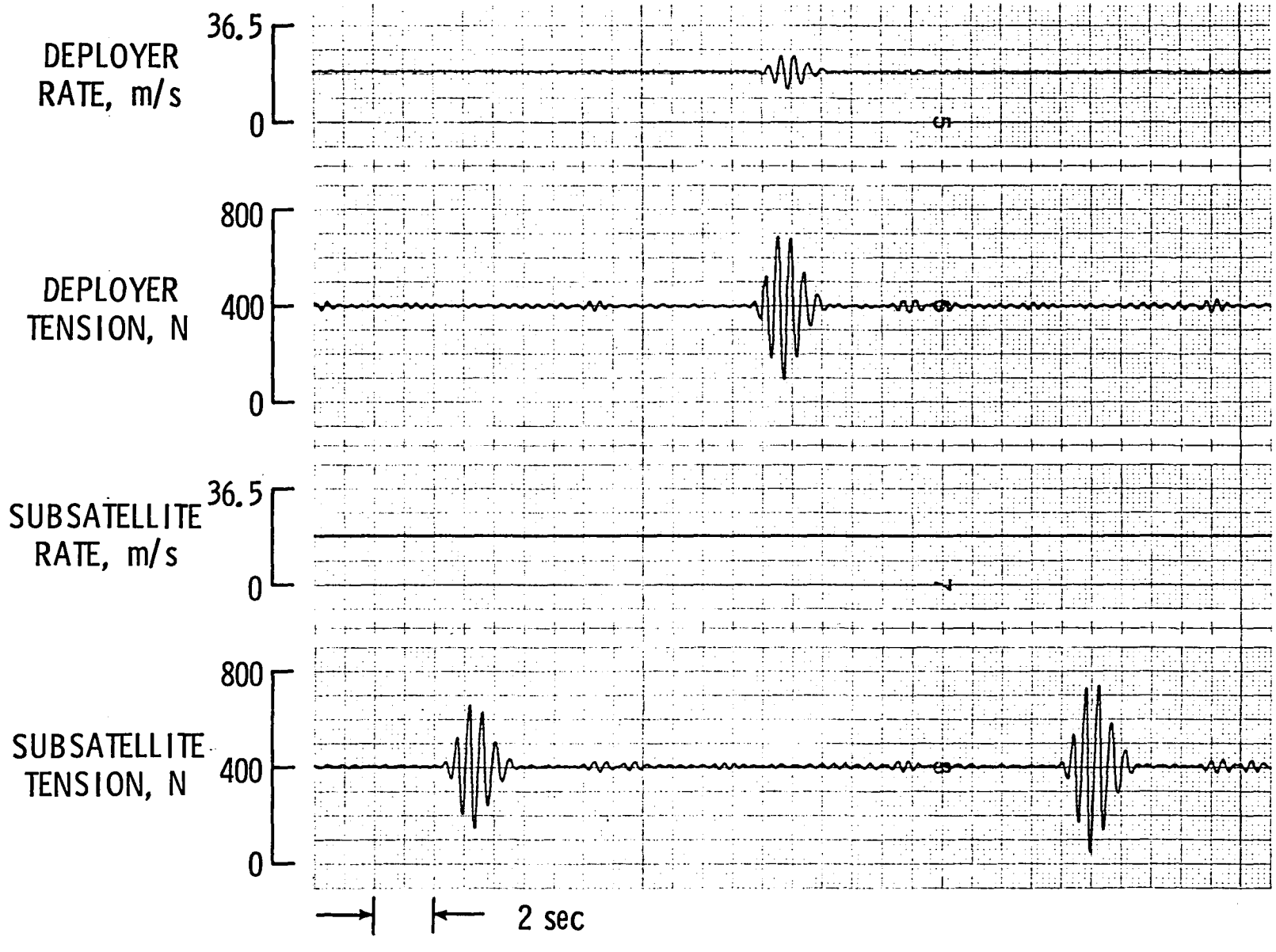

Figure 5.- Tension Vibrations

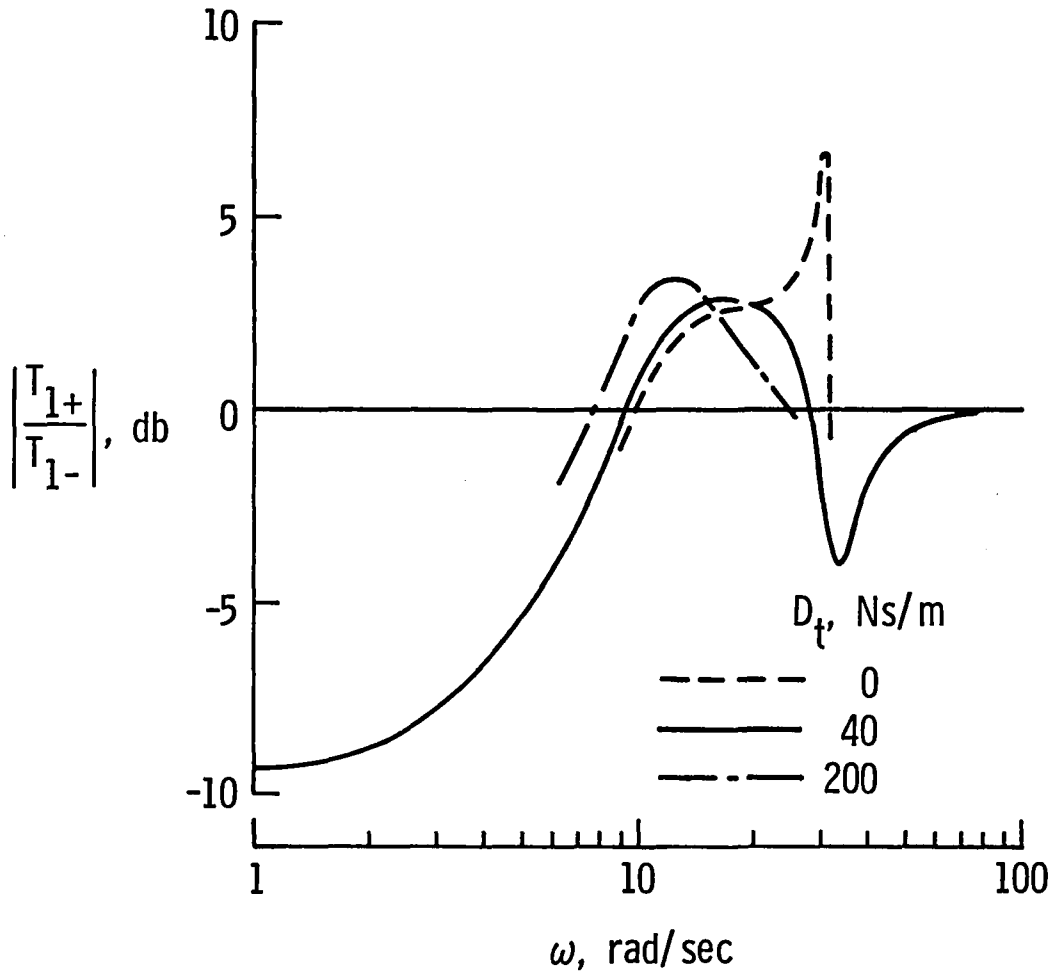

Figure 6.- Tension Wave Reflections at Deployer for Different Damping Coefficients of the Tension Sensor

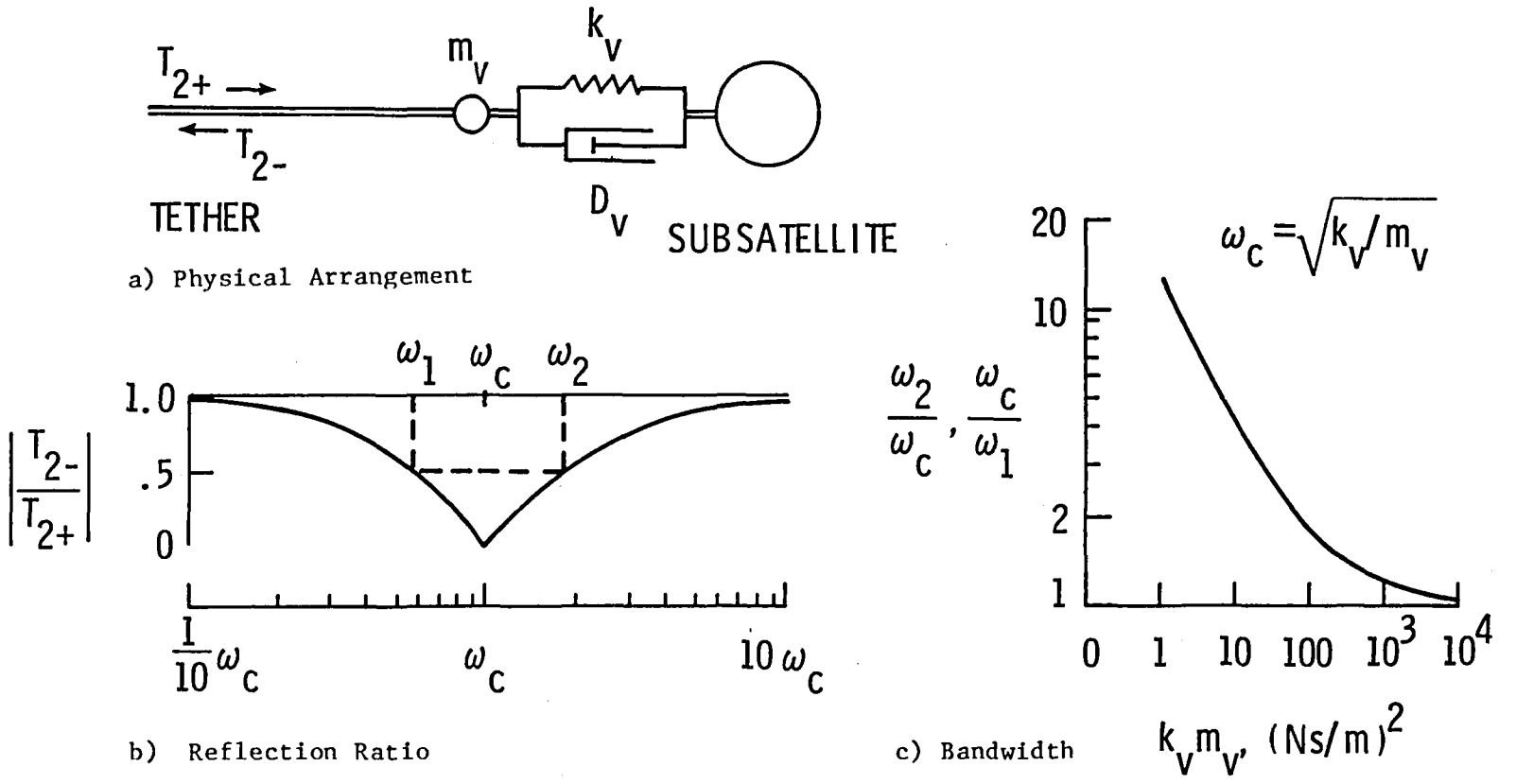

Figure 7.- Vibration Damper, $D_v = A\sqrt{\rho E} = 10.95$ Ns/m

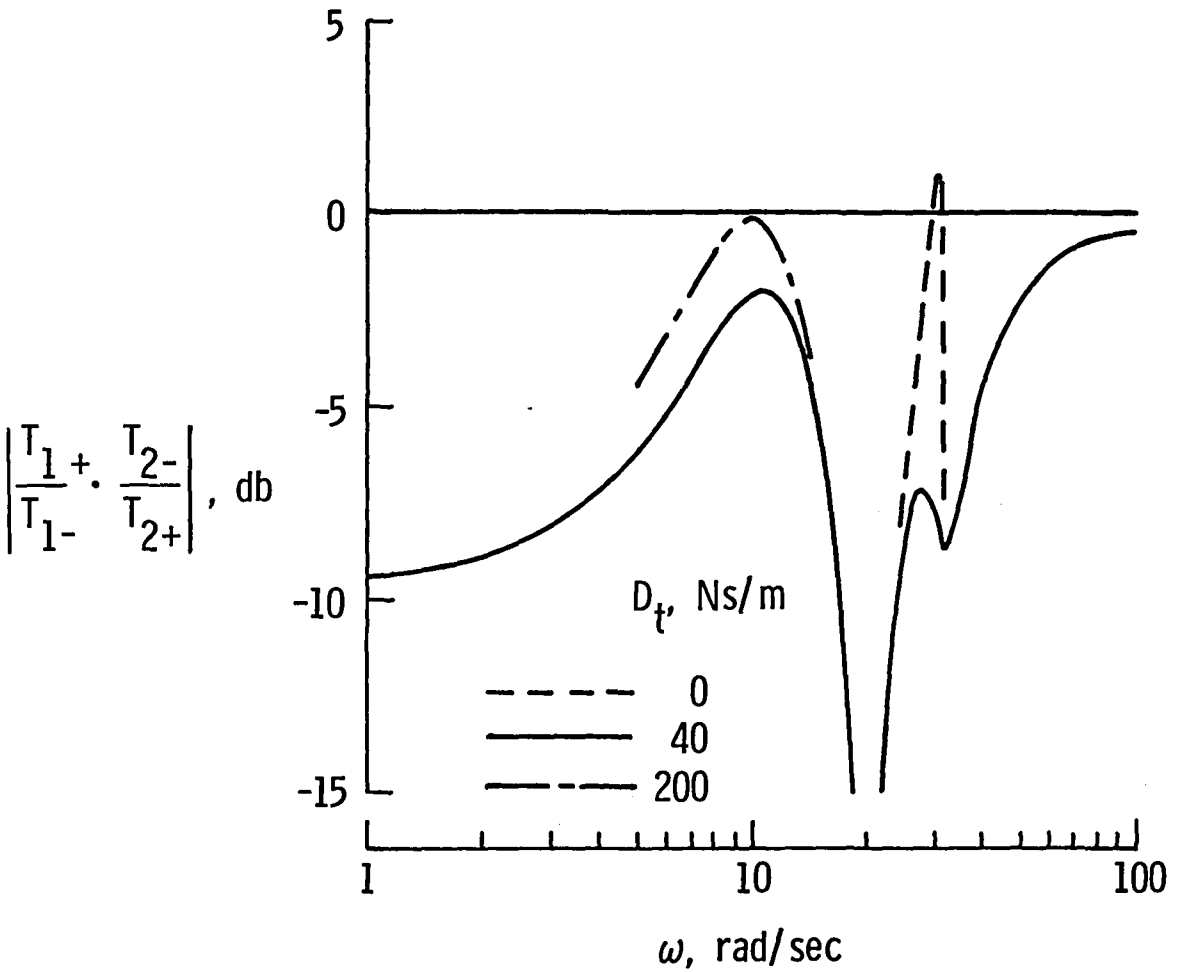

Figure 8.- Effect of Vibration Damper for Different Damping Coefficients of the Tension Sensor, $A\sqrt{\rho E}$ = 10.95 Ns/m, m_v = .79 kg, k_v = 316 N/m

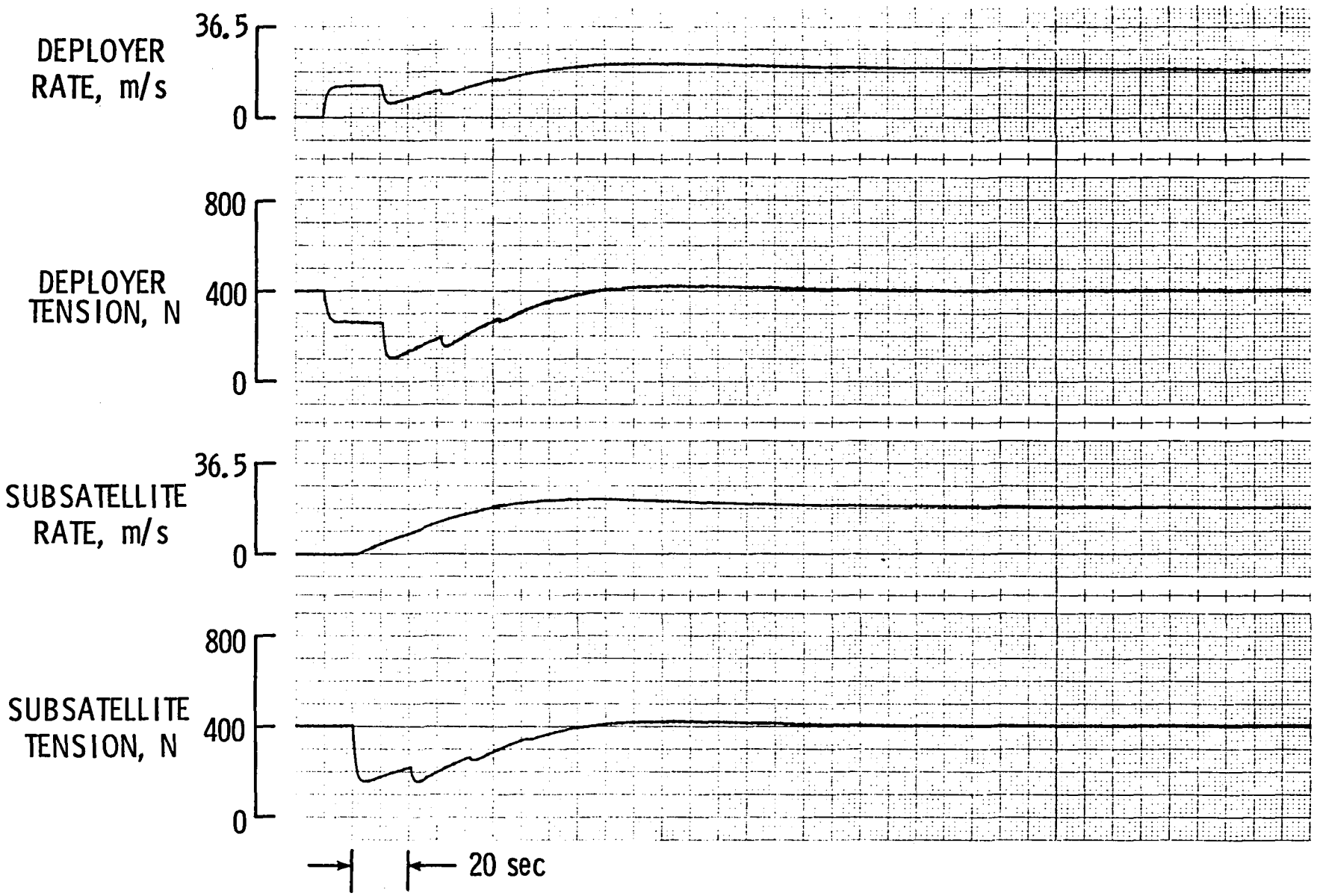

Figure 9.- Vibration Damper Effectiveness

1. Report No.	2. Government Accession No.	3. Recipient's Catalog No.
NASA TM-85799		

4. Title and Subtitle	5. Report Date
Tension Waves in Tethered Satellite Cables	May 1984
	6. Performing Organization Code: 505-34-03-02
7. Author(s): Frederick J. Lallman	8. Performing Organization Report No.
	10. Work Unit No.
9. Performing Organization Name and Address: NASA Langley Research Center, Hampton, VA 23665	11. Contract or Grant No.
	13. Type of Report and Period Covered: Technical Memorandum
12. Sponsoring Agency Name and Address: National Aeronautics and Space Administration, Washington, DC 20546	14. Sponsoring Agency Code

15. Supplementary Notes

16. Abstract

A one-degree-of-freedom simulation of the Tethered Satellite System (TSS) was programed using a distributed system model of the tether based on the one-dimensional wave equation. This model represents the time varying tension profile along the tether as the sum of two traveling waves of tension moving in opposite directions. A control loop was devised which combines a deployment rate command with the measured tension at the deployer to produce a smooth, stable rate of deployment of the subsatellite. Simulation results show a buildup of periodic bursts of high frequency oscillation in tension. This report covers the mathematical modelling and simulation results and explains the reason for the observed oscillations. The design of a possible vibration damping device is discussed.

17. Key Words (Suggested by Author(s))		18. Distribution Statement
Tethered Satellites	Tetherlines	Unclassified - Unlimited
Wave Equation	Travelling Waves	
Vibrations	Dynamic Stability	Subject Category 18
Vibration Dampers		

19. Security Classif. (of this report)	20. Security Classif. (of this page)	21. No. of Pages	22. Price
Unclassified	Unclassified	23	A02

For sale by the National Technical Information Service, Springfield, Virginia 22161